Journal of Applied Electrochemistry (2006) 36:239–247
DOI 10.1007/s10800-005-9054-2

Structures, physicochemical properties and oxygen reduction activities of carbons derived from ferrocene-poly(furfuryl alcohol) mixtures

JUN-ICHI OZAKI[1,*], KIYOMI NOZAWA[1], KUNITAKA YAMADA[1], YOSHINORI UCHIYAMA[1], YOKO YOSHIMOTO[1], ATSUYA FURUICHI[1], TOMONARI YOKOYAMA[1], ASAO OYA[1], L.J. BROWN[2] and J.D. CASHION[2]
[1]*Department of Nano-Material Systems, Graduate School of Gunma Universty, 1-5-1, Tenjin-cho, Kiryu, Gunma, 376-8515, Japan*
[2]*Department of Physics, Monash University, Clayton, Victoria, 3168, Australia*
*(*author for correspondence: tel.: +81-277-30-1351, fax: +81-277-30-1353, e-mail: jozaki@chem.gunma-u.ac.jp)*

Received 4 January 2005; accepted in revised form 31 August 2005

Key words: catalytic carbonization, ferrocene, oxygen reduction, poly(furfuryl alcohol), shell-like carbon, turbostratic carbon

Abstract

The structure, physicochemical properties and oxygen reduction abilities of carbons prepared by the carbonization of mixtures of ferrocene and poly(furfuryl alcohol) were studied. X-ray diffraction (XRD), Raman spectroscopy and transmission electron microscopy (TEM) studies revealed that the carbons thus prepared consisted of two components; amorphous and turbostratic shell-like components. The fraction, f_{sharp}, obtained by the analysis of the (002) peak in XRD was found to be a parameter that represented the degree of formation of the shell-like components. The formation of the shell-like components induced an increase in the mesopore volumes. Electrical conductivity increased exponentially with f_{sharp}, which indicated that the conduction process was governed by a percolation process of the conductive shell-like components. The amount of CO-desorption by O_2-TPD technique showed a maximum desorption at $f_{sharp} = 0.3$, and the further development in the sharp component led to a decrease in the CO-desorption. Mössbauer spectroscopy technique revealed the presence of α-Fe, γ-Fe, $Fe_{1-x}O$ and Fe_3C in the prepared carbons, which were soluble species to acids. The oxygen reduction activity was studied in a oxygen saturated sulfuric acid solution by rotating disk electrode voltammetry. The oxygen reduction potential varied with f_{sharp}; initially it increased by $f_{sharp} = 0.3$ and then it decreased at higher f_{sharp} values. This behavior was similar to that of CO-desorption, which meant the presence of an adequate degree of the development of the shell-like structure for maximizing oxygen adsorption. Removal of the surface metal component from the carbons by acid-washing resulted in no decrease in the oxygen reduction activities of the carbons. The nature of the active sites on the carbon materials is discussed.

1. Introduction

The basic structure of carbon materials is stacked graphenes, of which the configuration varies from a regularly ordered one such as found in graphite to a randomly oriented one as observed for amorphous carbons [1]. Physicochemical properties of carbons, such as adsorption capacity, electrical conductivity and chemical reactivity, etc., are known to be influenced by the basic structures.

Carbonization is a process that converts organic compounds to carbon materials, which occurs by heat-treatment up to approximately 1000 °C. This comprises the following processes: elimination of heteroatoms such as hydrogen, oxygen, nitrogen and sulfur from the original organic compounds, formation and fusion of aromatic rings to form graphenes and commencement of the alignment of the graphenes to some extent. Another aspect of the carbonization is a process to construct π-electron systems [2, 3]. Indeed, the electrical conductivity of the carbons increased by ten orders of magnitude during carbonization from 400 °C to 1000 °C, which can be explained in terms of the increase in size of the graphenes [3].

We have been studying the designing rules to prepare carbon materials with desired properties, particularly by means of controlling the carbonization process. For this purpose, we have utilized the catalytic effects of hetero-atoms toward the carbonization [4–6]. Transition metals such as iron, nickel and cobalt are known to be active for carbon gasification [7], carbon deposition [8], and catalytic graphitization [9]. In our previous study, carbons prepared from the mixtures of ferrocene and poly(furfuryl alcohol) were found to promote electron

transfer in a redox reaction of ferricyanide ion [6]. The same effect was also observed when a phenol–formaldehyde resin [10] was used as the organic materials for carbon. The electrocatalytically active carbons commonly showed fur-like structures under SEM [6] and the formation of T_s-carbons by XRD measurements [11]. T_s-carbons are the carbons that show resistance against graphitization even by heat treatment at 3000 °C, which were named by Oya et al., since they are thermally stable turbostratic carbons [9].

The proton exchange membrane fuel cell (PEMFC) is an attractive device for power supply for automobiles, domestic power generation and portable electronics, due to its inherent advantages of high energy density, cleanliness and low working temperature [12]. The low working temperature, however, induces a serious problem in the cathode reaction [13]; i.e. an increase in the cathode overpotential.

In order to accelerate the oxygen reduction rate, a considerable amount of platinum catalyst is used, which is one of the obstacles impeding the commercialization of PEMFC. A number of ideas have been proposed to reduce the amount of the platinum as follows: improvement of platinum loading procedures [14, 15], enhancement of the activity by alloying platinum with other cheaper metals [16], improvement of the dispersion of platinum particles by using novel nanocarbon materials, and developments of non-platinum catalysts [17–20]. Much attention had been devoted to electrocatalysis of oxygen reduction to carbon materials; however the challenges still remain to reduce the overpotential of oxygen electrodes in fuel cells [21].

The electroreduction of a dioxygen molecule includes both chemisorption and electron transfer on the electrode surface. It is interesting to know whether the T_s-carbons that showed excellent activities for a simple electron transfer reaction, a redox reaction of ferrycyanide, are also effective for the electroreduction of oxygen, or not. The objectives of the present study are to obtain detailed knowledge on the structural and physicochemical natures of the T_s-carbons and to examine their electrochemical oxygen reduction activities.

2. Experimental

2.1. *Sample preparation*

The samples prepared are listed in Table 1 along with their preparation conditions. A predetermined amount of ferrocene (Wako Pure Chemical, purity >98%) was dissolved in warmed furfuryl alcohol (Wako Pure Chemical, purity >97%), where the ratios of ferrocene to furfuryl alcohol were determined so as to give 1 or 2 mass% Fe in the final carbon products. Polymerization of the furfuryl alcohol was done in an electric oven at 80 °C for 72 h in nitrogen atmosphere, by using conc. HCl as initiator. The polymerized sample was carbonized at 700 °C for 1 h in a helium stream at a heating rate of 2.5 °C min^{-1} by using an infrared image furnace (RHL-E410P, Shinku Riko Co. Ltd.). The sample was cooled at 250 °C min^{-1} after carbonization. The carbonized samples are referred to by putting "c" in front of the nominal iron content, for example, cFe(1) stands for the carbon sample with 1 mass% of nominal iron content. Samples with longer carbonization time 10 h, cFe(1)-L, or with slower cooling rate 2 °C min^{-1}, cFe(2)-S, were also prepared. A sample without ferrocene was also prepared as a control, by employing the normal conditions, i.e. 1 h carbonization time and 250 °C min^{-1} cooling rate. This is denoted as cFe(0). The above samples were pulverized and were used in further investigations.

cFe(1) and cFe(2) were acid-washed with 6 M H_2SO_4 in order to observe the effect of the iron species on the catalytic activities of the carbons. The acid-washing treatment was carried out by immersing the samples in H_2SO_4 solution with stirring. Every hour for the first few hours the solution was replaced with fresh acid solution until no color was observed in the supernatant solution. After continuous stirring of the samples overnight in the acid solution, the samples were then thoroughly rinsed with fresh distilled water repeatedly, until the solution became neutral. The samples were then ready for the electrochemical measurements after drying.

2.2. *Characterization*

The obtained carbons were characterized by X-ray diffraction (XRD), transmission electron microscopy (TEM), N_2 adsorption, electrical conductivity, ^{57}Fe Mössbauer spectroscopy and oxygen adsorption TPD (temperature programmed desorption).

XRD patterns were obtained by an X-ray diffractometer (RINT2100/PC, Rigaku Corp.) for the powder samples that were charged into a shallow dip of a glass sample holder. The X-ray source was Cu-Kα with an operation condition of 30 kV and 20 mA.

TEM observation was done for the ground sample by putting it on a grid coated with carbon film. Transmission electron microscope (JEM2010, JEOL) was operated at an acceleration voltage of 200 kV.

Table 1. Sample preparation conditions, actual iron contents and f_{sharp} values

Sample	[a]Fe/mass %	[b]Time/h	[c]Rate/°C	[d]Fe/mass %	f_{sharp}/–
cFe(0)	0	1	250	0	0
cFe(l)	1	1	250	1.2	0.09
cFe(l)-L	1	10	250	1	0.40
cFe(2)	2	1	250	2	0.18
cFe(2)-S	2	1	1	2	0.29

[a]initial iron loading.
[b]carbonization time.
[c]cooling rate after carbonization.
[d]actual iron loading in the carbons measured by TG.

N_2 adsorption isotherms were obtained at liquid nitrogen temperature with an automatic apparatus (BELSORP 28SA, Japan BEL Co. Ltd.). Before the measurements, the samples were evacuated at 200 °C for 2 h. BET analysis and D-H analysis were applied to the isotherms in order to obtain surface areas and mesopore volumes.

Electrical conductivies of the powder samples were measured by the two-electrode method with a cylinder-piston type electrode assembly described elsewhere [22]. The applied pressure was fixed at 2 MPa where steady values were obtained. The conductivity was calculated from the resistance, the diameter of the electrode (5 mmϕ) and the distance between the two electrodes.

For the measurement of ^{57}Fe Mössbauer spectroscopy, the samples were charged into a Perspex® holder with 10 mm diameter. The amount of the sample was adjusted to several milligrams of iron atom per square centimeter. The source of γ-ray was ^{57}CoRh. The spectra were acquired at room temperature by a conventional constant acceleration spectrometer. Normally good quality spectra were obtained by overnight acquisition.

TPD measurements were conducted using equipment consisting of a quartz-glass sample tube with a thermocouple, a PID temperature controller, a quadrupole mass detector and a computer for the data collection (TPD-44, BEL Japan, Inc.). Five milligrams of the sample were charged into the tube to satisfy the differential reaction conditions, in order to avoid secondary desorption processes. The sample was initially heated in a helium stream up to 700 °C, and was kept at this temperature for 0.5 h. The sample was cooled down to 40 °C in the same gas flow, and then the gas flow was switched to 5%O_2-He mixture gas to make the sample to adsorb oxygen onto its surface by keeping the flow for 0.5 h. After the gas was switched to helium again, the sample was heated up to 700 °C at a rate of 20 °C min^{-1} with monitoring the emitting gas by the mass detector.

2.3. *Electrochemical methods*

The ORR activities of the obtained carbons were examined by rotating disk electrode voltammetry at room temperature, where oxygen saturated 1 M H_2SO_4 solution was used as the electrolyte. Five milligrams of the ground carbon was mixed with Nafion® solution (50 μl) (Aldrich) and ethanol (Wako Pure Chemicals) and ion-exchanged water (150 μl each) under ultrasonication to make a catalyst ink. One ml of the catalyst ink was applied on a glass-like carbon disk electrode (3 mmϕ). After evaporating the solvents, the ORR voltammograms were recorded by sweeping the potential from the rest potential to −0.1 V versus Ag/AgCl at 0.5 mV s^{-1} and 1500 rpm using electrochemical equipment (Electrochemical Analyzer Model 700A, ALS Co. Ltd.).

3. Results

3.1. *Structures of carbons*

Figure 1 shows the X-ray diffraction patterns of the selected samples. Different diffraction patterns were observed depending on the preparation conditions. For example, the carbon sample prepared without ferrocene, cFe(0), showed three broad diffractions at 23°, 42° and 79°, which are assigned to (002), (10) and (11) diffractions of amorphous carbons, respectively. In the case of the carbons prepared in the presence of ferrocene, development of (002) diffraction of carbon is observed at $2\theta = 26.1°$. Additional small peaks were also observed at 36.0, 41.4, 60.3 and 44.4°. The first three diffraction peaks were assigned to iron oxides denoted by $Fe_{1-x}O$ and the last one to ferrite.

The shapes of the (002) diffraction peaks of cFe(2) and cFe(1)-L were asymmetric, which could be separated into two different contributions, sharp component and broad component, as already reported previously [11]. The diffraction angle of the former was $2\theta = 26.1°$, which corresponded to turbostratic carbon, of which the stacking orders of graphenes were lost. The ratio of the peak area of the sharp peak to the total area of the (002) region was defined in order to represent the degree of development of the turbostratic phase as mentioned in the previous paper [11]. The values are also listed in Table 1. It was observed that the increases in the content of ferrocene and the residence time at higher temperatures led to formation of turbostratic carbon.

The dimensions of carbon crystallites, L_c and L_a were obtained by applying Scherrer's formula to the (002) and (11) diffractions, respectively. Figure 2 shows the dependence of the L_c and L_a on f_{sharp}. An increase in L_c from 1 nm to 1.5 nm was observed, when the f_{sharp} value increased from 0 to 0.09; however, no changes were observed for further increase in the f_{sharp} value. The L_a value, on the other hand, showed a steady increase with the increase in the f_{sharp} value as shown in Figure 2. It should be noted that a rapid increase in L_a was observed when the f_{sharp} value increased from 0.29 to 0.4. To sum up, the development of the turbostratic structure

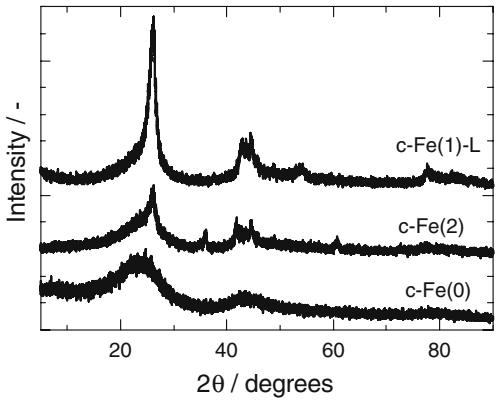

Fig. 1. X-ray diffractograms of the prepared carbons.

occurred in the enlargement of the graphene rather than the increase in the stacking numbers of the graphenes.

Figure 3 shows the Raman spectra of the carbons. The carbon prepared without adding ferrocene, cFe(0), only gave a spectrum with a low signal-to-noise ratio, which indicated that the carbon structure had not been established sufficiently. The carbons prepared in the presence of ferrocene showed the following changes with the increase in f_{sharp}. First, the D-band at 1360 cm^{-1} became sharper and more intense comparable to the G-band at 1600 cm^{-1}. Second, the changes can be found in the shapes of the G-band; i.e. the cFe(1) ($f_{sharp} = 0.09$) showed a symmetrical shape. However the shape became asymmetrical with increase in f_{sharp}, where another contribution was found at approximately 1580 cm^{-1} as a small hump. In general, the band at 1600 cm^{-1} corresponds to an aromatic C=C vibration of

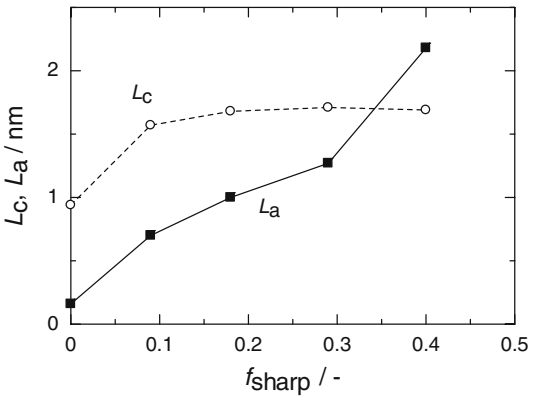

Fig. 2. Changes in the crystallite sizes of carbons, L_c and L_a, with f_{sharp}.

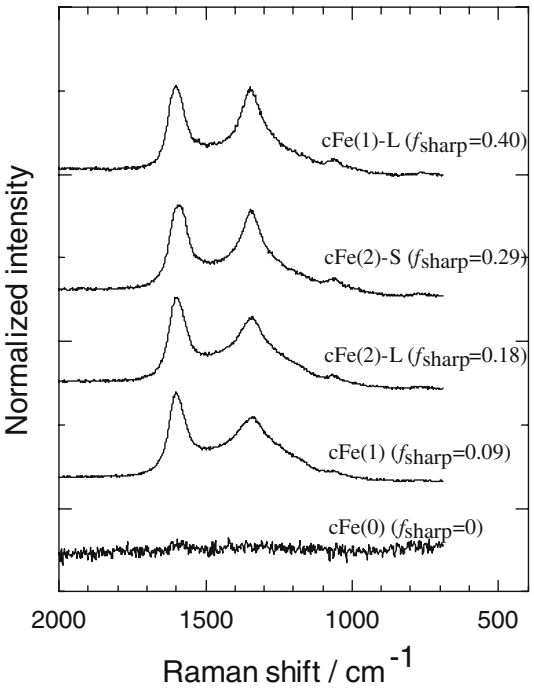

Fig. 3. Raman spectra of the carbonized samples.

organic materials. When the degrees of carbonization and graphitization increase, the band becomes sharper, and simultaneously the peak position shifts from 1600 cm^{-1} to 1580 cm^{-1}. This is a sign of the formation of carbon structures. In conclusion, the carbons prepared in the presence of ferrocene included two contributions: a disorganized organic part responsible for the 1600 cm^{-1} band and a well-ordered graphitic part responsible for the 1580 cm^{-1} band.

Figure 4 shows a part of the TEM images of the samples. The cFe(0) sample showed dotty structures that were characteristic of amorphous carbons. Curved shell-like structures were observed for the samples prepared in the presence of ferrocene. The probability of observing these structures increased with f_{sharp}. The stacking structure of carbon was observed as shown in the insert of Figure 4(d), which is a magnified image of the shell-like carbon. Similar shell-like structures had been observed, when carbon materials were prepared in the presence of cobalt or nickel instead of iron [23]. Our preliminary study of electron diffraction (ED) of the shell-like carbons revealed that the interlayer spacing d_{002} obtained from the ED agreed with the d_{002} obtained from the sharp components in XRD. Consequently, the sharp diffraction component in XRD could be identified as the shell-like carbons under TEM. From the above discussion, the defined f_{sharp} can be taken as the parameter representing the degree of the development of the shell-like carbons in the materials.

3.2. *Physicochemical properties of carbons*

Figure 5 shows the dependence of the BET surface area and the mesopore volume of the carbons on the development of shell-like carbon, f_{sharp}, which were calculated from nitrogen adsorption isotherms of the carbons. The cFe(0) sample had a BET surface area of about 200 $m^2\ g^{-1}$. With the increase in f_{sharp}, the BET surface area decreased once and then it turned to an increasing trend afterward. Since the BET surface area is dominated by the presence of micropores, the behavior indicated the collapse of micropores in the earlier stages of the shell-like carbon formation, and then the pore formation occurred again.

The mesopore volume also showed a small decrease at $f_{sharp} = 0.09$; however the extent was not as large as that for micropores. Further increase in f_{sharp} induced an increase in the mesopore volume, showing a maximum at $f_{sharp} = 0.09$. The addition of cobalt or nickel to furan resin resulted in the formation of mesopores in the carbonized samples, although the data have not been published yet. These results indicated a parallelism between the formation of the shell-like carbons and the mesopores. The spaces between the discrete shell-like units may be responsible for the mesopores.

Figure 6 shows the dependence of electrical conductivity of the powder carbon samples on f_{sharp}. The electrical conductivity increased exponentially with f_{sharp}. The highest conductivity was observed for

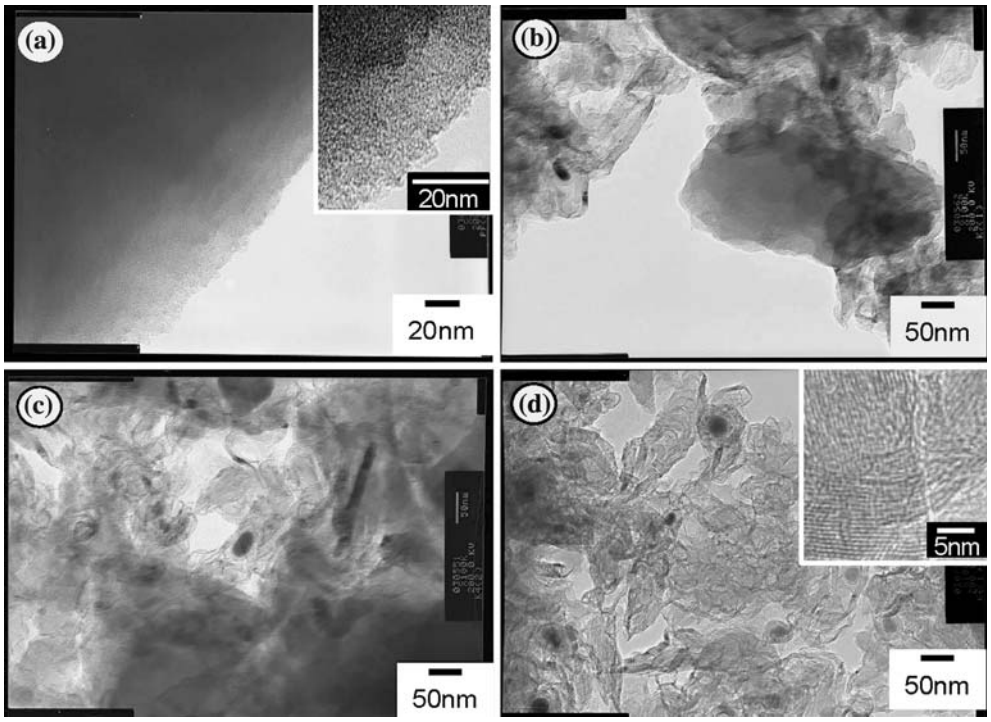

Fig. 4. Transmission electron microscopy images of the prepared samples. (a) cFe(0), (b) cFe(1), (c) cFe(2)-S, (d) cFe(1)-L. (a) and (d) included the magnified images in the inserts.

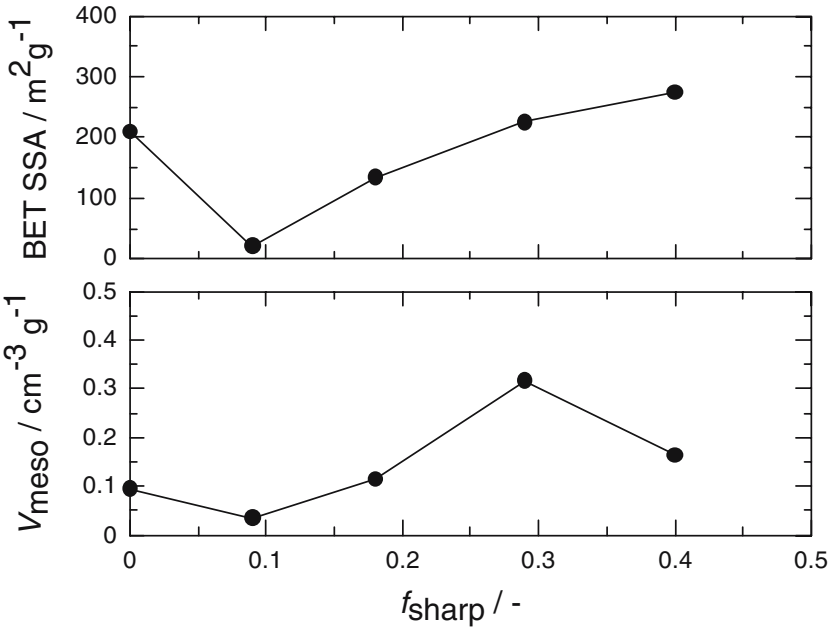

Fig. 5. Changes in the BET specific surface area and the mesopore volume with f_{sharp}.

cFe(2)-S, which is higher than that of cFe(0) by four orders of magnitude. The large increase in the electrical conductivity is partially due to the increase in L_a as shown in Figure 2, which led to enhancement of the density and the mobility of the π-electrons [3, 24]. The exponential relationship between the electrical conductivity and f_{sharp} indicated that the conduction process in these carbon materials was governed by a percolation process, where the electrical conduction takes place via the conduction paths formed by the connection of the shell-like components [25].

The active surface area of carbon is the surface area determined by oxygen adsorption, which has a profound correlation with the chemical reactivity of carbons [26]. In the present study, we obtained similar information on the oxygen adsorption site by using a TPD technique. Carbon monoxide was detected as the major desorbed gas from the present samples. The amount of desorbed

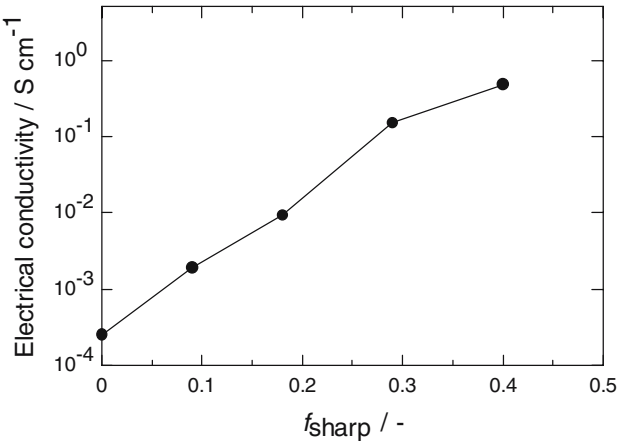

Fig. 6. Changes in the electrical conductivities of the carbonized samples with f_{sharp}.

carbon monoxide was plotted against f_{sharp} in Figure 7. The amount of carbon monoxide increased with f_{sharp} up to $f_{sharp} = 0.29$, and then decreased. This meant that the formation of the shell-like structure led to the formation of oxygen adsorption sites; however, excessive formation of the shell-like structure induced reduction in the number of sites.

3.3. *Chemical states of iron incorporated in carbon*

Mössbauer spectroscopy is a powerful technique to provide chemical information on iron species irrespective of their crystallinity. Figure 8 shows the Mössbauer spectra of the selected carbon samples. The parameters are listed in Table 2. The shapes of the spectra clearly depend on f_{sharp}. The sample with the lowest f_{sharp}, cFe(1), had dominant singlet absorption with an isomer shift of 0.1 mm s^{-1} wrt α-Fe. This was identified as an iron oxide ($Fe_{1-x}O$). With increase in f_{sharp} we observed the development of two sextets. These were identified as cementite ($\delta = 0.2$ mm s^{-1} and $B = 20$ *T*) and α-Fe ($\delta = 0$ mm s^{-1} and $B = 33$ *T*). γ-Fe was also observed at $\delta = -0.1$ mm s^{-1} in these spectra, although its intensity was not so large.

Figure 9 shows the formation of an iron species that was identified by Mössbauer spectrometry. The fractions of α-Fe and γ-Fe were independent of f_{sharp}. In contrast, wüstite and cementite varied with f_{sharp} in the opposite manner; wüstite decreased gradually and finally it disappeared from $f_{sharp} = 0.29$ to 0.4. Cementite, on the other hand, gradually increased up to $f_{sharp} = 0.29$ and showed a rapid increase from $f_{sharp} = 0.29$ to 0.4. Consequently, Mössbauer spectroscopy revealed that the iron species included in the present samples are metallic, oxides, and carbides, which are soluble in acidic conditions.

3.4. *O_2-reduction activity*

Figure 10 shows the hydrodynamic voltammograms for oxygen reduction, when the carbons were used as working electrodes. The cFe(0) sample showed an increase in reduction current that started approximately at 0.1 V versus Ag/AgCl, when the potential was negatively swept. The cFe(1), whose f_{sharp} was 0.09 showed almost the same trace as the cFe(0) sample. Both cFe(2) and cFe(2)-S samples showed increases in the onset potentials of the reduction current and also in the currents at more negative potential regions. However, cFe(1)-L which has the largest f_{sharp} in the present study, showed reduced current to the same level of cFe(1). For further discussion, the reduction potential, E_{O2}, is defined as the potential where the reduction current density of -10 μA cm^{-2} is reached.

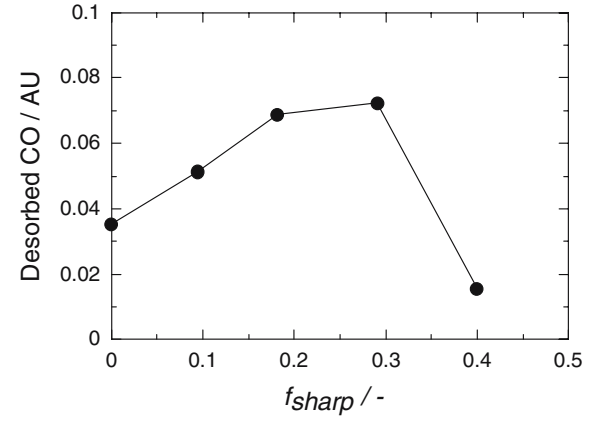

Fig. 7. Changes in the CO-dosorption determined by O_2-TPD with f_{sharp}.

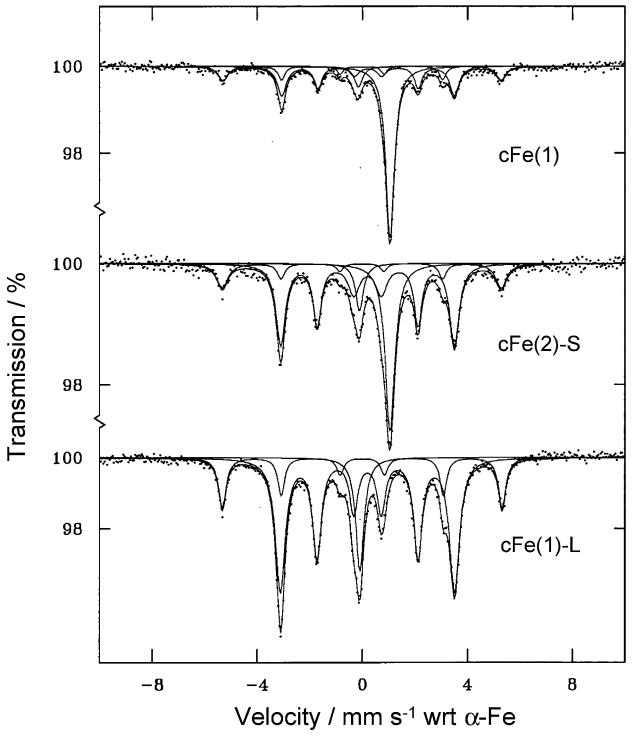

Fig. 8. Mösbauer spectra of the selected samples.

Table 2. Mössbauer parameters

Sample	f_{sharp}/–	$Fe_{1-x}O$		Fe_3C			α-Fe			γ-Fe	
		δ/mm s^{-1}	Area/%	δ/mm s^{-1}	B/T	Area/%	δ/mm s^{-}	B/T	Area/%	δ/mm s^{-}	Area/%
cFe(l)	0.09	1.04	46	0.21	20.3	31	−0.02	32.8	17	−0.17	6
cFe(l)-L	0.4		0	0.18	20.4	68	−0.01	32.7	16	−0.1	16
cFe(2)	0.18	1.05	33	0.2	20.3	42	−0.01	32.5	15	−0.12	10
cFe(2)-S	0.29	1.1	4	0.19	20.3	73	−0.02	32.8	17	−0.09	6

The relation between E_{O2} and f_{sharp} is given in Figure 11. The oxygen reduction potential increased up to $f_{sharp} = 0.29$ and then decreased. This suggests that the formation of shell-like carbons is required in order to show oxygen reduction activity; however, excess formation of the shell-like carbon resulted in a decrease in the activity.

A similar f_{sharp}-dependence was obtained for the CO-desorption measured by O_2-adsorption TPD as shown in Figure 7. In this figure, the amount of the CO-desorption of cFe(1) ($f_{sharp} = 0.09$) was larger than that of cFe(0); however, the oxygen reduction activities of these samples were almost the same. Here we have to consider the effect of electrical conductivity of the catalyst material, since the electrochemical current is dependent both on the electrical conductivity and the active sites for oxygen adsorption. The lower oxygen reduction activity for cFe(1) ($f_{sharp} = 0.09$) must be determined by its lower electrical conductivity.

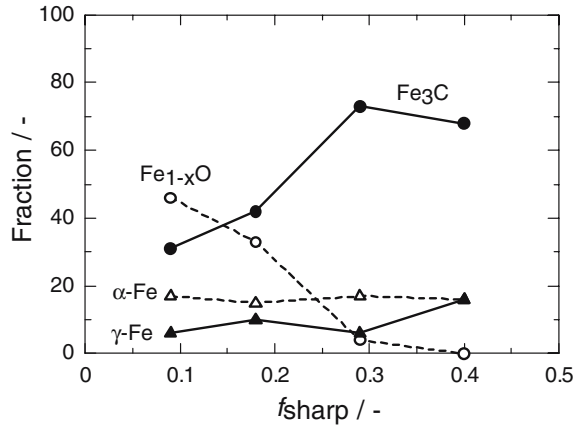

Fig. 9. Dependence of the iron-species determined by Mösbauer measurements on f_{sharp}.

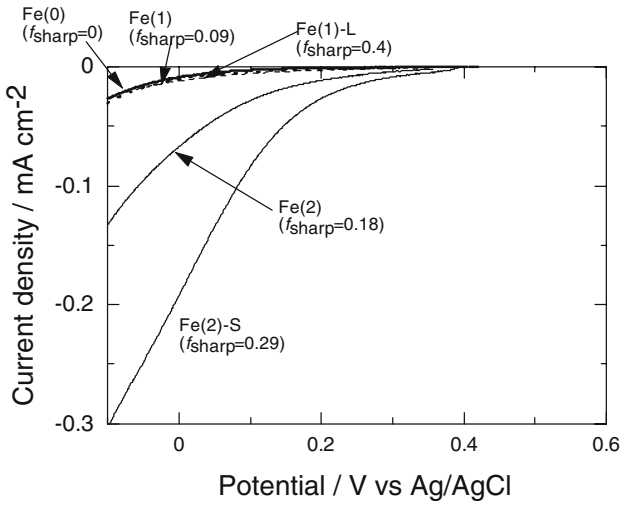

Fig. 10. Hydrodynamic voltammograms of the prepared carbons, when they were used as working electrodes for oxygen reduction in 1 M H_2SO_4 electrolyte. The voltammograms were obtained by rotating the electrode at a speed of 1500 rpm.

4. Discussion

What is the origin of the oxygen reduction activity introduced by the addition of ferrocene to the carbonizing systems? There seem to be two possibilities for the active sites in the present systems; one is sites formed on the carbon surfaces which adsorb oxygen molecules, and the other is iron-related sites. Pyrolysis of the phthalocyanine or porphyrin complexes adsorbed on carbon blacks is known to result in the formation of an oxygen reduction catalyst. Four major explanations for the activity have been proposed: (1) metal particles formed during pyrolysis [27, 28], (2) carbon surfaces influenced by the metal species [29], (3) N_4–M surface complexes formed by partial decomposition of N_4–metal complexes [30–32], (4) M–N–C surface complexes [33–37]. The most plausible candidate is now considered to be (4). Further, it has also been reported that the active surface complexes can be formed not only from N_4–M complexes such as phthalocyanines or porphyrins, but

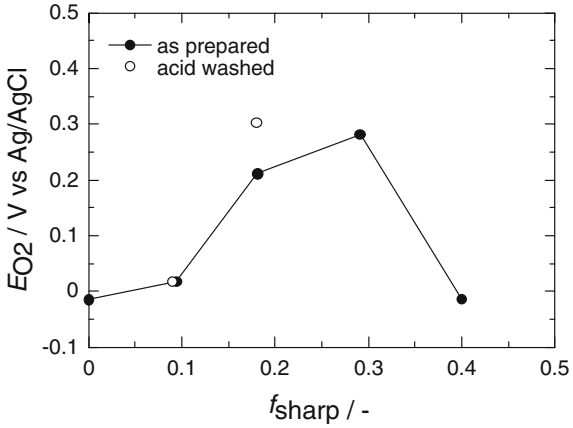

Fig. 11. Relation between the oxygen reduction potential, electrocatalytic activity, and the development degree of the nanoshell carbons.

also by adding sources of metals and nitrogen to the carbon substrate separately [35–37]. One chemical structural model of the surface complexes is a metal atom coordinated to the quinoline-like nitrogen formed by utilizing the edge site of the carbon substrate [38, 39].

Recently, Maldonado et al., prepared a carbon nanofiber from iron–phthalocyanine and demonstrated its activity for electrochemical oxygen reduction [40]. They considered that the activity originated from the surface functionalities located on the edges of the carbon nanofibers. The oxygen reduction activity of the nitrogen atoms located on the edge sites of the carbon materials has been reported by us [41]. Thus, we have to consider the possibility of the incorporation of nitrogen atoms on the carbon surfaces, since our polymerization and carbonization processes were carried out in a nitrogen stream. X-ray photoelectron spectroscopy measurements were performed on cFe(1) and cFe(1)-S samples, and no nitrogen was observed on their surfaces within the XPS detection limit.

In order to demonstrate that the oxygen reduction activities of our samples are not caused by the presence of the metal species on the surface, acid-washing was carried out on selected samples. The iron content of cFe(1) ($f_{sharp} = 0.09$) and cFe(2) ($f_{sharp} = 0.18$) decreased from 1.2 mass% to 0.9 mass% and from 2 mass% to 1.6 mass%, respectively. The reason for the incomplete removal of iron species is related to the presence of iron species encapsulated by carbon shells, which are stable even acid-washing. Indeed, many researchers have pointed out the formation of these structures [31, 32, 34, 42]. In the present case, the oxygen reduction activity did not decrease following acid-washing as represented by open symbols in Figure 11. This result was interpreted as due to the opening of pores that had been covered by the metal species, which gives more space to the reactant molecules. Detailed analysis is being undertaken in our laboratory.

Other possible candidates for the oxygen reduction activity are (1) iron oxides or hydroxides located in micropores and (2) the nature of the shell-like carbons. Acid-washing was performed by immersing the carbon samples in a 6 mol dm^{-3} H_2SO_4 solution overnight and exchanging the acid solution every hour for the first several hours. Since the time-scales are quite different between the acid-washing treatment and the electrochemical activity measurement, it is difficult to consider the possibility of the slowly diffused oxygen molecules deep into the micropore to be catalyzed by an insoluble iron species such as iron hydroxides located there.

According to He et al. [43], nickel has no activity for oxygen reduction. If this is so, the carbons prepared in the presence of nickelocene instead of ferrocene will not show oxygen reduction activity. We reported the formation of shell-like carbon and the electrochemical activity of the nicklocene-derived carbons [44]. Hence, our carbon materials may have a different mechanism for the activation of oxygen from the conventional transition metal complex-based catalyst systems. The main difference between the present and the conventional systems is the formation of carbons. In the conventional materials, metal-complexes were added onto the already-carbonized solids, such as carbon blacks or PTCDA derived carbons; however, in the present case, carbon materials were formed under the influence of the metal complexes. Because the organic materials, in our case of poly(furfuryl alcohol), are usually more reactive than carbon materials, there is a possibility for them to be chemically affected by the metal species during carbonization. There still remains the possibility that an extremely active iron-related species on the carbon promotes oxygen reduction, although these species can not be detected by usual XPS techniques. We consider that the major factor for the electrocatalytic activity relates to the nature of the shell-like carbons.

5. Conclusion

We investigated the structure, physicochemical properties and oxygen reduction activity of the carbons prepared from mixtures of ferrocene and poly(furfuryl alcohol). The following conclusions were obtained.

(1) XRD, Raman spectroscopy and TEM indicated the presence of two carbon phases, amorphous and turbostratic components, in the carbons prepared in the presence of ferrocene. In particular, TEM clearly showed the formation of shell-like structures. Comparison of the results of TEM and XRD concluded that the parameter f_{sharp}, defined as the fraction of the turbostratic component in (002) diffraction, represented the degree of the development of the shell-like structures.

(2) The increase in f_{sharp} resulted in the development of both mesopores and electrical conductivity. The electrical conductivity increased exponentially with f_{sharp}, indicating a percolation process. Mössbauer spectroscopy indicated that only acid-soluble iron species were included in the carbons. The density of oxygen adsorption sites on the carbons was evaluated using an O_2-adsorption temperature programmed technique (TPD). This showed an increase up to $f_{sharp} = 0.29$ and then a decrease at higher f_{sharp} values.

(3) Catalytic activity for the electroreduction of oxygen in acidic media were evaluated by rotating disk electrode voltammetry. The carbons containing shell-like structures showed larger catalytic activity than the carbon without shell-like structures. However, the activity did not simply increase with f_{sharp}; it showed a maximum at $f_{sharp} = 0.29$, where the maximum O_2 adsorption was obtained in the TPD analysis. The catalytic activity did not decrease, when the iron species were removed by acid-washing.

Comparing our present results with previous results on N_4–M catalysts, we tentatively conclude that the activity observed in the present study is due to the nature of the shell-like carbons. We are undertaking further work to understand the essence of the nature of the shell-like carbons.

Acknowledgements

This study was conducted as a project of the Research and Development of Polymer Electrolyte Fuel Cell, entrusted by the New Energy and Industrial Technology Development Organization (NEDO), (2002–2004 fiscal years). LJB and JDC received a grant from the Australian Research Council to conduct the Mössbauer measurements.

References

1. R.E. Franklin, *Proc. Roy. Soc. London* **A209** (1951) 196.
2. F. Carmona and P. Delhaes. Physical properties of non-crystalline carbons, *in* P.L. Walker Jr. and P.A. Thrower (Eds), Chemistry and Physics of Carbon 17, (Marcel-Dekker, New York, 1981), pp. 89.
3. S. Mrozowski, *Phys. Rev.* **85** (1952) 609.
4. J. Ozaki, T. Watanabe and Y. Nishiyama, *J. Phys. Chem.* **97** (1993) 1400.
5. J. Ozaki and Y. Nishiyama, *J. Appl. Phys.* **77** (1995) 4459.
6. J. Ozaki, M. Mitsui and Y. Nishiyama, *Tanso*, (1994) 268.
7. Y. Nishiyama, *Fuel. Proc. Technol.* **29** (1991) 31.
8. Y. Nishiyama and Y. Tamai, *CHEMTECH* **680** (1980) 1980.
9. A. Oya and H. Marsh, *J. Mater. Sci.* **17** (1982) 309.
10. J. Ozaki, M. Mitsui and Y. Nishiyama, *Carbon* **36** (1998) 131.
11. J. Ozaki, K. Nozawa and A. Oya, *Chem. Lett.* **1998** (1998) 573.
12. X. Wang, I.-M. Hsing and P.L. Yue, *J. Power Source* **96** (2001) 282.
13. J.H. Tian, F.B. Wang, Z.H.Q. Shan, R.J. Wang and J.Y. Zhang, *J. Appl. Electrochem.* **34** (2004) 461.
14. M. Uchida, Y. Furuoka, Y. Sugawara, H. Ohara and A. Ohta, *J. Electrochem. Soc.* **145** (1998) 3708.
15. S. Hitomi, H. Yasuda and M. Yamachi, *Electrochemistry* **73** (2005) 416.
16. T. Toda, H. Igarashi and M. Watanabe, *J. Electroanal. Chem.* **460** (1999) 258.
17. H. Jahnke, M. Shonbor and G. Zimmermann, *Top. Curr. Chem.* **61** (1976) 133.
18. D.A. Scherson, A.A. Tanaka, S.L. Gupta, D. Tryk, C. Fierro, R. Holze, E.B. Yeager and R.P. Lattimer, *Electrochim. Acta* **31** (1986) 1247.
19. F. Jaouen, S. Marcotte, J.P. Dodelet and G. Lindbergh, *J. Phys. Chem. B* **107** (2003) 1376.
20. M. Bron, S. Fiechter, P. Bogdanoff and H. Tributch, *Fuel Cells* **2** (2002) 137.
21. K. Kinoshita, *Carbon – Electrochemical and Physicochemical Properties* (Wiley Interscience Publication, New York, 1988) p. 360.
22. J. Ozaki and Y. Nishiyama, *J. Appl. Phys.* **65** (1989) 2744.
23. P.B. Hirsch, *Proc. Roy. Soc. London A* (1954) 226.
24. J. Ozaki, A. Furuichi and A. Oya, 'Preparation of electrochemically active carbons for oxygen reduction by carbonization of mixtures of metal complexes and furan rResin', Extended Abstract of Carbon 2004, Providence, USA July 11–16 (2004).
25. P.L. Waters, 'Proceedings of the 5th Conference on Carbon', (edited by S. Mrozowski, Vol. 2, p. 131, Pergamon, New York, 1963).
26. F.G. Emmerich, J.C. Soysa, I.L. Torriani and C.A. Luengo, *Carbon* **25** (1987) 417.
27. N.R. Laine, F.J. Vastola, P.L. Walker Jr and R.G. Jenkins, *J. Phys. Chem.* **67** (1963) 2030.
28. L. Dignard Bailey, M.L. Trudeau, A. Joly, R. Schulz, G. Lalande, D. Guay and J.P. Dodelet, *J. Mater. Res.* **9** (1994) 3203.
29. M.C. Martines-Alves, J.P. Dodelet, D. Guay, M. Ladouceur and G. Tourillon, *J. Phys. Chem.* **96** (1992) 10898.
30. G. Gruenig, E.G. Jaeger, U. Moeller and K. Wiesener, *Z. Phys. Chem (Leipzig)* **267** (1986) 994.
31. J.A.R. van Veen, J.F. van Baar and K.J. Kroese, *J. Chem. Soc. Faraday Trans, 1* **77** (1981) 2827.
32. G. Faubert, G. Lalande, R. Cote, D. Guay, J.P. Dodelet, L.T. Weng, P. Bertrand and G. Denes, *Electrochim. Acta* **10** (1996) 1689.
33. L.T. Weng, P. Bertrand, G. Lalande, D. Guay and J.P. Dodelet, *Appl. Surf. Sci.* **84** (1995) 9.
34. G. Lalande, G. Tamizhmani, R. Cote, L. Dignard-Bailey, M.L. Trudeau, R. Shulz and D. Guay, *J. P. Dodelet, J. Electrochem. Soc.* **142** (1995) 1162.
35. A. Widelov and R. Larsson, *Electrochim. Acta* **37** (1992) 187.
36. J. Fournier, G. Lalande, R. Cote, D. Guay and J.P. Dodelet, *J. Electrochem. Soc.* **144** (1997) 218.
37. G. Lalande, R. Cote, D. Guay, J.P. Dodelet, L.T. Weng and P. Bertrand, *Electrochim. Acta* **42** (1997) 1379.
38. R. Cote, D. Guay, J.P. Dodelet and G. Denes, *J. Electrochem. Soc.* **145** (1998) 2411.
39. M. Lefevre, J.P. Dodelet and P. Bertrand, *J. Phsy. Chem.* **B106** (2002) 8705.
40. S. Maldonado and K.J. Stevenson, *J. Phsy. Chem. B* **108** (2004) 11375.
41. J. Ozaki, T. Anahara, A. Furuichi and A. Oya, Electrocatalytic activity of B-/N-doped carbon particles for the reduction of oxygen molecule, Extended Abstracts of Carbon 2003, Oviedo, Spain 6–10, July (2003).
42. M. Ladouceur, G. Lalande, D. Guay, J.P. Dodelet, L. Dignard-Dailey, M.L. Trudeau and R. Shulz, *J. Electrochem. Soc.* **140** (1993) 1974.
43. P. He, M. Lefevre, G. Faubert and J.P. Dodelet, *J. New Mater. Electrochm. Systems* **2** (1999) 243.
44. K. Kawata, Y. Otake, A. Furuichi, J. Ozaki and A. Oya, Preparation of metal-doped carbons from phenol–formaldehyde resin and their electrocatalytic activities for oxygen reduction, Preprint of 30th Annual Meeting of the Carbon Society of Japan, Chiba, Japan, Dec. 4–6 (2003), pp. 12–13.